

1 **PPAR- γ in macrophages limits pulmonary inflammation and promotes host recovery following**
2 **respiratory viral infection**

3
4 Su Huang^{a, b}, Bibo Zhu^{a, b}, In Su Cheon^{a, b}, Nick P. Goplen^a, Li Jiang^{a, b}, Ruixuan Zhang^a, R. Stokes
5 Peebles Jr.^c, Matthias Mack^d, Mark H. Kaplan^b, Andrew H. Limper^a and Jie Sun^{a, b, #}

6
7 ^aThoracic Diseases Research Unit, Division of Pulmonary and Critical Care Medicine, Department of
8 Medicine, Department of Immunology, Mayo Clinic College of Medicine and Science

9 ^bHB Wells Pediatric Research Center, Department of Pediatrics, Indiana University School of Medicine

10 ^cDepartment of Medicine, Vanderbilt University Medical Center

11 ^dDepartment of Nephrology, University Hospital Regensburg, Germany

12
13 Running title: PPAR- γ regulates influenza diseases and recovery

14
15 #Corresponding author: Jie Sun, Sun.Jie@mayo.edu.

16 S Huang and B Zhu contributed equally to this work

17

18

19

20

21

22

23

24

25

26

27 **ABSTRACT**

28 Alveolar macrophages (AM) play pivotal roles in modulating host defense, pulmonary inflammation and
29 tissue injury following respiratory viral infections. However, the transcriptional regulation of AM
30 function during respiratory viral infections is still largely undefined. Here we have screened the
31 expression of 84 transcription factors in AM in response to influenza A virus (IAV) infection. We found
32 that the transcription factor PPAR- γ was downregulated following IAV infection in AM through type I
33 interferon (IFN)-dependent signaling. PPAR- γ expression in AM was critical for the suppression of
34 exaggerated antiviral and inflammatory responses of AM following IAV and respiratory syncytial virus
35 (RSV) infection. Myeloid PPAR- γ deficiency resulted in enhanced host morbidity and increased
36 pulmonary inflammation following both IAV and RSV infections, suggesting that macrophage PPAR- γ is
37 vital for restricting severe host disease development. Using approaches to selectively deplete recruiting
38 monocytes, we demonstrated that PPAR- γ expression in resident AM was likely important in regulating
39 host disease development. Furthermore, we showed that PPAR- γ was critical for the expression of wound
40 healing genes in AM. As such, myeloid PPAR- γ deficiency resulted in impaired inflammation resolution
41 and defective tissue repair following IAV infection. Our data have suggested a critical role of PPAR- γ
42 expression in lung macrophages in modulating pulmonary inflammation, the development of acute host
43 diseases and the proper restoration of tissue homeostasis following respiratory viral infections.

44

45 **IMPORTANCE:** Respiratory viral infections, like IAV and respiratory syncytial virus (RSV) infections,
46 impose great challenges to the public health. Alveolar macrophages (AM) are lung resident immune cells
47 that play important roles in protecting the host against IAV and RSV infections. However, the underlying
48 molecular mechanisms by which AM modulating host inflammation, disease development and tissue
49 recovery are not very well understood. Here we identify that PPAR- γ expression in AM is crucial to
50 suppress pulmonary inflammation and diseases, and to promote fast host recovery from IAV and RSV
51 infections. Our data suggest that targeting macrophage PPAR- γ may be a promising therapeutic option in
52 the future to suppress acute inflammation and simultaneously promote recovery from severe diseases
53 associated with respiratory viral infections.

54

55

56

57

58

59

60 **INTRODUCTION**

61 Acute respiratory viral infections, such as influenza A virus (IAV) and respiratory syncytial virus (RSV)
62 infections, cause severe morbidity and mortality, and are among leading causes of death in children and
63 the elderly (1, 2). Particularly, IAV virus infection kills ~500,000 people globally and up to 50,000 people
64 in the United States each year (3). In addition to seasonal outbreaks, pandemic IAV viruses occasionally
65 emerge and can cause catastrophic illness and widespread death. Current strategies for IAV prevention
66 and treatment include yearly vaccination and anti-viral drugs. However, frequent changes in the surface
67 antigens of IAV virus due to antigenic shift and drift can allow IAV to escape antibody-mediated
68 immunity following vaccination (4, 5). Anti-viral treatment is generally only effective during a very short
69 time period early after IAV infection. Furthermore, many circulating IAV strains have developed
70 resistance to the current antiviral drugs (6). Thus, there is urgent need to better understand the
71 pathophysiology and the protective immune responses to IAV infection for the development of future
72 preventive and therapeutic means.

73

74 The disease pathogenesis associated with IAV infection results from a combination of the deleterious
75 effects of virus replication and the host innate and adaptive immune response associated with control and
76 ultimately clearance of virus (7, 8). The major contribution of the host response to lung injury during IAV
77 infection is exemplified by the immune-mediated lung inflammation and injury associated with infections
78 with the 1918 pandemic IAV or the highly pathogenic H5N1 avian IAV. The inability to control the host
79 responses in these infections results in excessive inflammatory cell infiltration into the lungs and
80 overproduction of pro-inflammatory mediators ((9, 10).

81

82 As important components of innate immunity, tissue macrophages and monocyte populations are
83 heterogeneous multifunctional immune sentinel cells important in modulating tissue homeostasis,
84 inflammation, injury and repair (11-15). The main macrophage population in the respiratory tract is
85 alveolar macrophages (AM) that play important roles in lung homeostasis and pulmonary anti-microbial
86 defense (16, 17). Compared to other tissue macrophages, monocytes and monocyte-derived cells, AM
87 have distinct functions and phenotypes that include high autofluorescence, low CD11b expression, and
88 high expression of CD11c and Siglec-F (16, 18). AM precursors develop mainly from fetal monocytes,
89 which seed the lung prior to birth, and massively expand and develop into mature macrophages in
90 response to GM-CSF and TGF- β after birth (18-20). A number of factors including PPAR- γ , mTORC1,
91 phosphoinositide kinase PIKfyve and L-plastin were also recently shown to be important in AM
92 development and function (19, 21-24). Interestingly, AM appear to be essential for the protection against

93 IAV and other respiratory viral infections (25-31) . To this end, AM were identified as a major cellular
94 source of the antiviral cytokines, type I interferons (IFNs) (29). Furthermore, AM can phagocytize virus
95 and virus infected cells, clear cellular debris and exudates, and protect alveolar type I cells (ATI) from
96 infection, thereby suppressing the development of lethal inflammation and injury during IAV infection
97 (25-31). AM, particularly AM undergoing alternative polarization (M2), have also been implicated in the
98 repair of damaged tissues following IAV infection (32). However, the underlying molecular mechanisms
99 regulating the protective function of AM against respiratory viral infections remain to be fully elucidated.

100

101 PPAR- γ is a nuclear transcription factor, usually forming heterodimer with RXR (retinoid X receptor)
102 which recruit different co-activators or co-repressors to form a complex binding to PPAR-responsive
103 regulatory elements in the genome to modulate the expression of genes involved in adipogenesis, lipid
104 metabolism and inflammation (33). PPAR- γ has been shown to be vital for M2 polarization and the
105 restriction of excessive production of inflammatory factors (34, 35), although the roles of PPAR- γ in
106 regulating macrophage inflammatory responses against viral infections have not been explored. AM
107 constitutively express high levels of PPAR- γ (19). Mice with *loxP*-flanked alleles encoding PPAR- γ
108 (*Pparg*^{fl/fl}) and with CD11c-driven expression of Cre recombinase (Cd11c-cre) that is efficiently
109 expressed in fetal monocytes, exhibit severe defects in the AM compartment, suggesting that PPAR- γ is
110 essential for AM development from fetal monocytes (19). Interestingly, prophylactic or therapeutic
111 treatment of mice with natural or synthetic ligands which activate PPAR- γ resulted in diminished host
112 morbidity and mortality during IAV infection (36-40) . However, the cellular and molecular mechanisms
113 by which PPAR- γ agonists promote host protection against IAV infection have not been defined. In
114 addition, the physiological and cell type-specific function of PPAR- γ in response to endogenous ligands
115 during IAV infection are currently unknown.

116

117 In this report, we demonstrated that PPAR- γ was down-regulated in AM via IFNs following IAV
118 infection. PPAR- γ repressed macrophage pro-inflammatory responses and promoted the expression of
119 wound healing gene programs independent of M2 polarization, thereby modulating lung inflammation,
120 host morbidity and tissue repair. We further showed that PPAR- γ expression and function in AM were
121 likely important in dictating host diseases and recovery from respiratory viral infection.

122

123

124

125 RESULTS

126 IAV infection downregulates PPAR- γ expression in macrophages through IFNs

127 AM are important in regulating antiviral immunity and injury. However, the molecular mechanisms
128 regulating AM responses to viral infection are still not well understood. To explore the transcriptional
129 regulation of AM responding to viral infection, we infected WT AM with IAV PR8 (IAV, 10 MOI) *in*
130 *vitro* and then determined the expression of 84 transcription factors (TFs) following overnight culture
131 using Qiagen RT²-PCR array. We found that a numbers of TFs involved in antiviral innate immunity were
132 upregulated, while several TFs including *Pparg* were downregulated in AM following IAV infection
133 (Figure 1 A and B). Quantitative PCR results also showed that *Pparg* was downregulated in AM
134 following IAV infection (Figure 1 C). Western blot analysis confirmed decreased PPAR- γ at the protein
135 level in IAV infected AM (Figure 1 D). To determine whether IAV infection downregulates *Pparg* in AM
136 *in vivo*, we sorted AM (CD11c⁺/Siglec F⁺) from the lungs of uninfected (day 0) or IAV-infected mice (4,
137 6, 10 or 15 days post infection (d.p.i.)) and examined *Pparg* expression by realtime RT-PCR (Figure 1 E).
138 We found that IAV infection diminished *Pparg* expression in AM, particularly at 6 d.p.i. (Figure 1 E).
139 Western blot analysis confirmed that AM isolated from IAV-infected mice (6 d.p.i.) exhibited decreased
140 PPAR- γ protein levels compared to AM isolated from uninfected mice (Figure 1 F). IAV infection
141 triggers the production of anti-viral cytokines type I IFNs by AM (6). We next examined whether type I
142 IFNs were involved in the regulation of PPAR- γ expression in AM. We found that IFN- α treatment
143 suppressed PPAR- γ expression in AM (Figure 1 G). Next, we infected AM with IAV and then blocked
144 type I IFN signaling with the inclusion of IFNAR1 blocking antibody (α -IFNAR1) in culture. We found
145 that α -IFNAR1 treatment abolished IAV-induced suppression of *Pparg* expression in AM (Figure 1H).
146 Similarly, α -IFNAR1 treatment abolished Poly IC induced suppression of *Pparg* expression in AM
147 (Figure 1H). Together, these data suggest that IAV infection inhibited PPAR- γ expression in AM
148 through IFN signaling. Consistent with the notion, we found that STAT1 could bind to *Pparg* locus
149 following IFN- α treatment, suggesting that STAT1 activation following IFN signaling may directly
150 modulate *Pparg* transcription in AM (Figure 1I).

151

152 PPAR- γ suppresses antiviral inflammation, but does not regulate M2 genes following infection

153 PPAR- γ is required for AM development because the deletion of PPAR- γ in CD11c⁺ cells (*Pparg*^{ACD11c})
154 resulted in impaired AM generation (Figure 2A and (19)). However, compared to CD11c-cre, *Lyz2*-cre
155 expression in fetal monocytes is incomplete (19). As the result, *Lyz2*-cre driven PPAR- γ deficiency
156 (*Pparg*^{ALyz2}) in AM resulted in relatively normal AM development (Figure 2A and (19)). In comparison to
157 the severe defects of AM development and maturation (evidenced by dramatic increase of CD11b (19))
158 observed in *Pparg*^{ACD11c} mice, *Pparg*^{ALyz2} mice had comparable percentages of AM and only slightly

159 increased CD11b expression compared to those of control mice, suggesting that AM development and
160 maturation were relatively normal in *Pparg*^{ALyz2} mice (Figure 2A). Nevertheless, *Lyz2*-cre is able to
161 mediate gene recombination in adult AM compartments and AM from adult *Pparg*^{ALyz2} mice exhibited
162 impaired PPAR- γ expression (Figure 2 B and (30)). We therefore used AM from littermate control
163 (*Pparg*^{fl/fl}, WT) or *Pparg*^{ALyz2} mice for our further analysis on the roles of PPAR- γ in regulating AM
164 function during respiratory viral infections. We first isolated AM from uninfected control or *Pparg*^{ALyz2}
165 mice, and infected the AM with IAV *in vitro* as in Figure 1. Following infection, WT and *Pparg*^{ALyz2} AM
166 showed relatively comparable levels of viability (data not shown). We then examined the expression of
167 type I IFNs, inflammatory cytokines and M2 genes in control or PPAR- γ -deficient AM following IAV
168 infection. We found that PPAR- γ deficiency enhanced the expression of *Ifna4*, *Ifnb1*, *Tnf*, *Il1b* and *Ccl2*
169 expression, but did not affect the expression of *Retnla* (encoding RELM- α protein) and *Arg1* (encoding
170 Arginase 1 protein) (Figure 2C). These data suggest that PPAR- γ suppressed AM antiviral and
171 inflammatory responses, but did not change macrophage polarization following IAV infection. We next
172 infected control or *Pparg*^{ALyz2} mice with IAV and then sorted AM from the lungs of infected mice at 1 or
173 3 d.p.i. We found that PPAR- γ deficient AM exhibited enhanced type I IFN and inflammatory gene
174 expression, but showed similar levels of *Retnla* and *Arg1* expression compared to those of control AM at
175 3 d.p.i. (Figure 2D). These data suggest PPAR- γ functioned to inhibit antiviral and inflammatory
176 responses, but did not regulate M2 polarization following IAV infection.

177

178 **Myeloid PPAR- γ suppresses lung inflammation, host morbidity and mortality**

179 To explore PPAR- γ expression in macrophages in regulating host antiviral responses and disease
180 development following IAV infection, we infected control or *Pparg*^{ALyz2} mice with IAV and examined
181 host mortality, morbidity, viral replication and inflammatory responses at different days post infection.
182 Compared to control mice, *Pparg*^{ALyz2} mice had enhanced host mortality and morbidity, and delayed
183 weight recovery following IAV infection (Figure 3 A, B). We examined the kinetics of IAV replication in
184 the respiratory tract using plaque forming unit (pfu) assay and found that *Pparg*^{ALyz2} mice exhibited
185 significant increased virus titers early days following IAV infection (4 d.p.i.) compared to control mice
186 (Figure 3C). However, *Pparg*^{ALyz2} mice had comparable viral titers at 7 d.p.i. and most of the mice cleared
187 their infectious virus around 10 d.p.i. (3 out of 11 mice exhibited detectable viruses in control or
188 *Pparg*^{ALyz2} bronchoalveolar lavage fluid (BAL)) (Figure 3 C). Thus, *Pparg*^{ALyz2} mice showed similar viral
189 clearance kinetics as control mice and suggest that the enhanced morbidity and mortality observed in
190 *Pparg*^{ALyz2} mice was not merely due to the failure of viral clearance. Consistent with the viral clearance

191 data, we found that *Pparg*^{ALyz2} mice exhibited comparable levels of IAV-specific CD8⁺ T cell responses
192 (both H2d^b NP₃₆₆₋₃₇₄ tetramer⁺ and H2d^b PA₂₂₄₋₂₃₃ tetramer⁺) at 7, 10 and 15 d.p.i. (Figure 3D).

193

194 Next, we measured lung inflammatory cytokine (CCL2 and TNF- α) levels in the BAL at different days
195 following IAV infection to determine whether *Pparg* expression in myeloid cells regulates pulmonary
196 inflammation. We found that *Pparg*^{ALyz2} mice had significant higher CCL2 and TNF- α levels at early days
197 post IAV infection (i.e. 1 or 3 d.p.i.) (Figure 3E). Notably, although the differences did not reach
198 statistical significance, *Pparg*^{ALyz2} mice showed trend of increased CCL2 protein levels in the BAL at 7,
199 10 or 15 d.p.i., indicating that *Pparg*^{ALyz2} mice may have modest increased pulmonary inflammation at
200 later days post infection. To this end, we used a more sensitive approach to examine inflammatory gene
201 expression in the lungs of control or *Pparg*^{ALyz2} mice by Qiagen RT²-PCR array. We found that lungs of
202 *Pparg*^{ALyz2} mice exhibited altered expression of inflammation-related genes including higher expression of
203 a number of pro-inflammatory genes (such as *Il6*, *Cxcl1* and *Fos*) at day 10 d.p.i. (Figure 3 F). Taken
204 together, these data suggest that myeloid PPAR- γ deficiency led to enhanced early viral replication,
205 exuberant inflammatory reaction and increased severity of host sickness.

206

207 **Myeloid PPAR- γ inhibits inflammation and morbidity during RSV infection**

208 To examine whether PPAR- γ controls AM inflammatory responses to other virus infection, we infected
209 isolated AM from control or *Pparg*^{ALyz2} mice with RSV, a virus that affects millions of children. Similar
210 to what we have observed following IAV infection (Figure 2C), we found that PPAR- γ deficiency
211 enhanced *Ifna4*, *Ifnb1*, *Tnf*, *Il1b* and *Ccl2* expression following RSV (line 19, 10 MOI) infection *in vitro*,
212 suggesting that PPAR- γ also controls antiviral and inflammatory responses against RSV infection (Figure
213 4A). We then infected control or *Pparg*^{ALyz2} mice with RSV (line 19) and examined host morbidity and
214 lung inflammatory responses. We found that myeloid PPAR- γ deficiency increased weight loss following
215 RSV infection (Figure 4 B). We also found that *Pparg*^{ALyz2} mice had enhanced inflammatory innate
216 immune cells (neutrophils and monocytes) present in the lungs at 4 d.p.i. (Figure 4C), suggesting that
217 *Pparg*^{ALyz2} mice had higher pulmonary inflammation compared to control mice. Consistently, BAL of
218 *Pparg*^{ALyz2} mice had higher TNF- α and IL-1 β levels compared to those of control mice at 4 d.p.i. (Figure
219 4D). Thus, myeloid PPAR- γ was required for the suppression of exuberant host inflammation and
220 exaggerated morbidity following RSV infection. These data suggest that macrophage PPAR- γ may
221 restrict host disease development in a broad spectrum of respiratory viral infections.

222 **PPAR- γ expression in resident AM is likely required for controlling host disease development**

223 Lysozymes are widely expressed in myeloid cells including neutrophils, monocytes and macrophages. We
224 crossed *Lyz2-cre* mouse with a cre reporter strain R26R-eYFP mouse to examine Cre deletion in the
225 myeloid compartment. In agreement with previous report (35), we observed *Lyz2-cre* activity in majority
226 of alveolar macrophages and neutrophils, partially in $CD11b^+$ monocytes/macrophages (Figure 5A).
227 Western-blot analysis on sorted myeloid cell populations isolated from the lungs revealed that AM
228 expressed high levels of PPAR- γ and lung $CD11b^+$ monocyte/macrophage population expressed
229 comparatively lower levels of PPAR- γ (Figure 5B), while neutrophils did not express detectable PPAR- γ ,
230 which is consistent with previous reports (35) (Figure 5B). To explore the potential roles of PPAR- γ in
231 regulating inflammation of AM, monocytes/monocyte-derived macrophages and/or epithelial cells, we
232 sorted AM, $CD11b^+$ monocytes/macrophages and $CD45^-$ (mainly epithelial cells) from IAV-infected
233 lungs of control or *Pparg^{ALyz2}* mice at 1 and 3 d.p.i. and examined inflammatory cytokine expression. We
234 found that elevated *Tnf* and *Ccl2* expression was mainly observed in AM, but not in $CD11b^+$
235 monocytes/macrophages nor in $CD45^-$ cells (Figure 5C). We next explored the relative contributions of
236 PPAR- γ in AM and monocytes/monocyte-derived macrophages in controlling host disease development
237 during IAV infection. To this end, we crossed *Pparg^{ALyz2}* mice to *Ccr2^{-/-}* mice to block monocyte traffic to
238 the infected lungs (40-43). We found that, compared to *Ccr2^{-/-}/Pparg^{fl/fl}* mice, *Ccr2^{-/-}/Pparg^{ALyz2}* mice lost
239 more weight and exhibited delayed recovery (Figure 5D), suggesting that enhanced disease development
240 in *Pparg^{ALyz2}* mice is independent of monocytes or monocyte-derived cells. We next assessed whether
241 treatment of anti-CCR2 (MC21 mAb), which selectively depletes recruiting monocytes (44) could affect
242 host morbidity in *Pparg^{ALyz2}* mice. As reported (43), MC21 treatment greatly decreased monocyte
243 infiltration to the lung (Figure 5E). However, MC21 treatment did not significantly alter host weight loss
244 in neither control nor *Pparg^{ALyz2}* mice (Figure 5F), again suggesting that monocytes are dispensable for
245 phenotypes observed in *Pparg^{ALyz2}* mice following IAV infection. Taken together, these data suggest that
246 PPAR- γ expression in AM, rather than in monocytes or monocyte-derived cells, is probably responsible
247 for the restriction of exaggerated pulmonary inflammation and the suppression of the development of
248 severe diseases following respiratory viral infection.

249

250 **Macrophage PPAR- γ promotes tissue repair**

251 Following the clearance of IAV, the inflammatory responses in the lung resolve and the damaged tissue
252 undergoing repair process to restore normal tissue homeostasis. AM are thought to be involved in the
253 tissue repair process following lung injury (32). We therefore examined whether PPAR- γ affects AM
254 tissue repair function. To this end, we isolated control or PPAR- γ -deficient AM from WT or *Pparg^{ALyz2}*
255 mice and performed Qiagen RT²-PCR array to determine wound healing gene expression. We found that

256 PPAR- γ deficiency resulted in impaired expression of a large numbers of wound healing-related genes
257 including epithelial and endothelial growth factors such as *Vegf*, *Egf* and *Fgf7* (Figure 6 A, B). A numbers
258 of factors involved in tissue remodeling including *Mmp7*, *Mmp9* and *Timp1* were also decreased in
259 PPAR- γ -deficient AM (Figure 6 A, B). These data suggested that PPAR- γ expression is important in
260 regulating wound healing and tissue repair function of AM.

261

262 Therefore, we examined whether *Pparg*^{ALyz2} mice had impaired tissue recovery *in vivo* following viral
263 clearance. To this end, we examined lung histopathology with Hematoxylin and Eosin (H&E) staining of
264 lung sections at 15 d.p.i., when infectious virus has been cleared from IAV infection (Figure 3C). We
265 found that *Pparg*^{ALyz2} mice still had significant higher proportions of the inflamed and/or damaged areas
266 that were not properly repaired at day 15 p.i., when mice already recovered most of their lost weight
267 (Figure 3B and 6 C). To further explore the roles of myeloid PPAR- γ in regulating lung inflammation
268 resolution and tissue repair, we first examined airway inflammatory cell content (monocytes and
269 neutrophils, reflection of lung inflammatory resolution). We found that *Pparg*^{ALyz2} mice exhibited higher
270 neutrophil numbers at 15 d.p.i., suggesting that *Pparg*^{ALyz2} mice had impaired pulmonary inflammation
271 resolution (Figure 6 D). We also measured total protein concentrations in the BAL (reflection of
272 endothelial/epithelial leakage) at different days following IAV infection and observed that *Pparg*^{ALyz2}
273 mice had drastically higher protein levels in the BAL compared to those of control mice at 15 d.p.i
274 (Figure 6 E). These data indicate that *Pparg*^{ALyz2} mice had impaired inflammation resolution and
275 decreased damage repair. In further support of this view, we examined alveolar type II (AT II) epithelial
276 gene expression in the lungs of control and *Pparg*^{ALyz2} mice as a surrogate of tissue recovery at 8, 10 or 15
277 d.p.i. We found that ATII specific genes, *Sftp* and *Abca3*, were comparable between control and
278 *Pparg*^{ALyz2} lungs at 8 d.p.i. However, lungs of *Pparg*^{ALyz2} mice exhibited lower *Sftp* and *Abca3*
279 expression compared to those of control mice at 10 or 15 d.p.i. (Figure 6 F), indicating that lungs of
280 infected *Pparg*^{ALyz2} mice had diminished ATII cell regeneration and lung recovery during viral clearance.
281 Taken together, these data suggest that PPAR- γ promoted AM tissue repair function and myeloid-
282 deficiency of PPAR- γ resulted in diminished inflammation resolution and impaired tissue recovery
283 following IAV infection.

284

285

286

287 **DISCUSSION**

288 The transcriptional regulation of lung macrophage responses against respiratory viral infections is largely
289 undefined. Here we identify that PPAR- γ expression in AM is vital for their proper responses during both
290 IAV and RSV infection. PPAR- γ is an anti-inflammatory transcription factor able to antagonize NF- κ B-
291 mediated cytokine production constitutively and in response to TLR ligand stimulation (45). Consistent
292 with the notion, we showed that PPAR- γ -deficient AM produced increased levels of both antiviral and
293 pro-inflammatory cytokines in response to IAV and RSV infection. Notably, AM constitutively express
294 high levels of PPAR- γ , which may help to maintain a tolerogenic environment in the lung during
295 homeostasis. However, AM can also rapidly produce inflammatory cytokines following microbial
296 challenge (17, 46). The down-regulation of PPAR- γ in AM may help the AM to rapidly respond to certain
297 microbial challenges and provide beneficial functions under certain conditions. Nevertheless, the
298 complete loss of PPAR- γ in macrophages caused exaggerated release of inflammatory mediators and
299 enhanced disease development *in vivo* following IAV and RSV infections. These data suggest that PPAR-
300 γ counter-regulates the pathogenic inflammatory responses *in vivo*, and acts to ensure the proper function
301 of lung macrophages during respiratory viral infections.

302

303 The differential functions of AM and recruited monocyte/macrophage populations during homeostasis
304 and disease conditions have only begun to be appreciated. During respiratory viral infections, circulating
305 monocytes infiltrate the lungs in a CCR2-dependent manner and can give rise to exudate or inflammatory
306 macrophages at the site of infection (42). These CCR2-dependent inflammatory monocytes and
307 monocyte-derived cells have been associated with the development of immunopathology, although these
308 cells also contribute to the normal antiviral responses as the blockage of their migration to the lung due to
309 CCR2 inhibition or deficiency impaired and/or delayed host viral clearance during RSV and IAV
310 infections (31, 40-42, 44). Notably, CCR2 deficiency or CCR2 blockade did not significantly change
311 overall host morbidity in PPAR- γ sufficient or deficient background in our experimental system than what
312 was reported before(31, 41), in which CCR2 deficiency significantly diminished host morbidity and
313 mortality. Variations in infection schemes, virus stocks and/or microbiota (46) may contribute to the
314 different results observed. However, our results are supported by the findings of Aldridge et al (40), in
315 which *Ccr2*^{-/-} deficient mice exhibited similar morbidity and mortality as WT mice following IAV
316 infection.

317

318 In contrast, lung resident AM are often beneficial to the host during respiratory viral infections as AM
319 depletion impairs host antiviral responses with concomitant development of severe lung injury during
320 respiratory viral infections (25-31). However, AM do release inflammatory mediators following viral
321 infections and thus may contribute to the development respiratory inflammation and/or injury if their
322 responses are not tightly regulated. Multiple lines of evidence present in this study suggest that PPAR- γ
323 expression in AM rather than in monocytes and/or monocyte-derived cells is important in controlling host
324 inflammation and subsequent disease development. First, AM expressed high levels of PPAR- γ compared
325 to monocytes and monocyte-derived cells. Furthermore, sorted AM rather than monocytes or monocyte-
326 derived cells exhibited increased inflammatory responses. Finally, disruption of monocyte recruitment
327 into the lungs by using anti-CCR2 or genetic CCR2 deletion did not majorly impact the outcome of IAV
328 infection in WT and myeloid PPAR- γ deficient mice, suggesting that PPAR- γ expression in monocytes
329 may be dispensable for the regulation of the development of severe diseases following respiratory viral
330 infection. Interestingly, PPAR- γ expression also regulated the wound healing function of AM and tissue
331 recovery through the promotion of various growth factors and tissue remodeling factors. Notably, PPAR- γ
332 deficiency did not result in decreased M2 gene expression in AM with or without IAV or RSV infection,
333 suggesting that PPAR- γ may regulate AM repair function independent of M2 polarization. Thus, PPAR- γ
334 is vital for the proper function of AM during respiratory viral infection by restricting their inflammatory
335 features and simultaneously promoting their repair roles.

336

337 Type I IFNs are widely recognized as host-beneficial, anti-viral cytokines. They lead to the transcription
338 of IFN-stimulated genes that aim to eliminate the virus and prevent its spread by promoting anti-viral
339 state in nearby cells (47). However, type I IFNs are also the key initiators of pulmonary inflammatory
340 responses during respiratory viral infections and thus their actions must also be finely balanced to
341 maximize viral clearance while inflicting minimal damage to the tissue (48). Indeed, the exaggerated
342 production of type I IFNs have been implicated in the development of exuberant pulmonary inflammation,
343 severe host morbidity and mortality following respiratory viral infections (44, 49, 50). In this report, the
344 enhanced type I IFN production was observed in PPAR- γ deficient AM, but the absence of PPAR- γ in
345 AM resulted in significantly increased viral titers at four days following IAV infection, suggesting that
346 the enhanced production of type I IFNs by PPAR- γ -deficient AM was not sufficient to diminish viral
347 replication in the lungs. The exact reasons underlying the phenomenon warrant further investigation.
348 Nevertheless, given the potential inflammatory function of type I IFNs, it is possible that the altered
349 production of type I IFNs along with the dysregulated inflammatory cytokine production in PPAR- γ
350 deficient AM contribute to the severe outcome of IAV infection in the myeloid PPAR- γ deficient mice.

351

352 In summary, our findings have uncovered critical roles of PPAR- γ in regulating inflammatory responses
353 of AM, the development of acute host disease and the proper restoration of tissue homeostasis following
354 respiratory viral infections. Further studies are warranted to examine the therapeutic potential of
355 modalities that can specifically modulate the expression of PPAR- γ in AM for the treatment of severe
356 respiratory viral infections and their associated pathologies.

357

358

359

360

361

362

363

364

365

366

367

368

369

370

371

372

373

374

375

376

377

378

379

380

381

382

383

384

385

386

387

388

389

390

391

392

MATERIALS AND METHODS

393 **Mouse and infection.** WT C57/BL6 mice were purchased from the Jackson Laboratory. *Lyz2-cre*,
394 *CD11c-cre*, *Pparg^{fl/fl}*, *R26R-eYFP*, *Ccr2^{-/-}* were purchased from the Jackson Laboratory and bred in house.
395 *Pparg^{ΔLyz2}* mice were generated by crossing *Pparg^{fl/fl}* mice with *Lyz2-cre* mice. *Pparg^{ΔCD11c}* were
396 generated by crossing *Pparg^{fl/fl}* mice with *CD11c-cre* mice. *Ccr2^{-/-} Pparg^{fl/fl}* and *Ccr2^{-/-} Pparg^{ΔLyz2}* mice
397 were generated by crossing *Pparg^{fl/fl}* or *Pparg^{ΔLyz2}* mice with *Ccr2^{-/-}* mice. *Lyz2-cre R26R-eYFP* reporter
398 mice were generated by crossing *R26R-eYFP* mice with *Lyz2-cre* mice. All mice housed in a specific
399 pathogen-free environment. For IAV infection, influenza A/PR8/34 strain (~200 pfu/mouse) was diluted
400 in FBS-free DMEM media (Corning) on ice and inoculated in anesthetized mice through intranasal route
401 as described before (51). Host mortality was determined based on humane endpoint (more than 30%
402 weight loss or moribund) or deaths before humanely sacrifice. For RSV infection, RSV (strain line 19,
403 ~5×10⁶ pfu/mouse) was diluted in FBS-free DMEM media (Corning) on ice and inoculated in
404 anesthetized mice through intranasal route as described (52).

405
406 **AM culture and infection *in vitro*.** AM were obtained from BAL. Briefly, alveolar lavages were pooled
407 from BAL washes from 3-5 mice (PBS with 2 mM EDTA) and stored on ice. Red blood cell lysis was
408 then performed in ACK lysis buffer (0.15 M NH₄Cl, 1 mM KHCO₃, 0.1 mM Na₂EDTA, pH 7.2) at room
409 temperature for 2 min. Freshly isolated cells were rested in complete medium (RPMI-1640, 10% FBS, 1%
410 Pen/Strep) for 4 h at 37°C and 5% CO₂. The non-adherent cells were discarded, and the plates were rinsed
411 with warm PBS. For AM infection *in vitro*, seeded cells were infected with or without 10 MOI of IAV
412 PR8 virus or RSV line 19 as indicated in the text for 1 hour and then cultured for overnight. For AM IFN
413 treatment *in vitro*, 10⁵ AM were plated in 12-well plate and treated with 50 ng/ml IFN-α (BioLegend) or
414 vehicle overnight in the presence of recombinant GM-CSF to keep AM alive (Biolegend, 10ng/ml). Cell
415 lysates were analyzed by quantitative RT-PCR or western blot.

416
417 **Quantitative RT-PCR.** mRNA from cultured AM (pooled from multiple mice), *in vivo* sorted AM
418 (pooled from multiple mice) or homogenates from individual lungs as indicated in the text was isolated
419 with Total RNA purification kit (Sigma) and treated with DNase I (Invitrogen). Random primers
420 (Invitrogen) and MMLV reverse transcriptase (Invitrogen) were used to synthesize first-strand cDNAs
421 from equivalent amounts of RNA from each sample. RT-PCR was performed with Fast SYBR Green
422 PCR Master Mix (Applied Biosystems). qPCR was conducted in duplicates in QuantStudio3 (Applied
423 Bioscience). Data were generated with the comparative threshold cycle (Delta CT) method by
424 normalizing to hypoxanthine phosphoribosyltransferase (HPRT). Sequences of primers used in the studies
425 are provided as follows. *Abca3*: TTCTGGTTCTCCGCTCTGTT, GTACATGAGGGGGATGATGG.

426 *Arg1*: CAATGAAGAGCTGGCTGGTG, TGAGCATCCACCCAAATGAC.
427 *Ccl2*: GTCACCAAGCTCAAGAGAGAGGTC, CCTACAGAAGTGCTTGAGGTGGTT.
428 *Hprt*: CTCCGCCGGCTTCCTCCTCA, ACCTGGTTCATCATCGCTAATC.
429 *Ifna4*: TCCATCAGCAGCTCAATGAC, AGGAAGAGAGGGCTCTCCAG.
430 *Ifnb1*: TCCACCAGCAGACAGTGTT, CTTTGCACCCTCCAGTAATAGC.
431 *Il1b*: GGGCCTCAAAGGAAAGAATC, TACCAGTTGGGGAACCTCTGC.
432 *Pparg*: TGCCAGTTTCGATCCGTAGA, ATGAATCCTTGGCCCTCTGA.
433 *Retnla*: TGCCCTGCTGGGATGACTGCT, GGACAGTTGGCAGCAGCGGG.
434 *Sftpb*: CTGTGCCAAGAGTGTGAGGA, TTGGGGTTAATCTGGCTCTG.
435 *Tnf*: CATGCGTCCAGCTGACTAAA, TCCCCTTCATCTTCCTCCTT.

436
437 **RT² Profiler PCR Array.** Total RNA from lung tissue or AM was extracted as described above. Equal
438 amount of total RNA was used for the synthesis of first strand cDNA with kit from Qiagen. First strand
439 cDNA was mixed with 2xFast SYBR Green Master Mix (Applied Bioscience) and water in a formula
440 directed in the manual. 25 µl of the mixture was added into each well of the 96 well plate provided by
441 manufacture. The wells in the plate include different primers in each well to detect 84 target genes,
442 housekeeping genes, negative and positive control genes. qPCR was conducted in QuantStudio3 (Applied
443 Bioscience). Obtained raw data was analyzed in software provided by Qiagen (accessible online on the
444 website of Qiagen). Following the instruction step by step, upload Excel file, designating control group,
445 select housekeeping gene to normalize result and calculate the relative expression quantity.

446
447 **Cell depletion.** For monocyte depletion, mice were treated intraperitoneally (i.p.) with anti-CCR2
448 antibody (clone: MC21, 25 µg/mouse in 200 µl of PBS)(53) or control IgG daily from day 0 to day 6.

449
450 **Lung histopathology.** Following euthanasia, mice were perfused with PBS (10 mL) via the right
451 ventricle. 10% paraformaldehyde (PF) was then gently instilled into the lung and left inflated for 1 minute
452 before excising and moving lobe to 10% PF for 48 hours followed by transfer to ethanol (70%). Samples
453 were shipped to Mayo Clinic Histology Core Lab (Scottsdale, AZ) where they were embedded in paraffin
454 and 5 µm sections were cut for Hematoxylin and eosin stain. To quantify percent of inflamed or disrupted
455 alveolar area, H&E slides were scanned through the Aperio whole slide scanning system and exported to
456 image files. Computer-based image analysis was performed using the Image J software (NIG, Bethesda,
457 MD, USA). We first determined the total lung area by converting the image into gray scale followed with
458 red highlighting through the adjustment of the Threshold. For determination of the inflamed and disrupted
459 area, color images were split into single channels. We then used the green channel, highlighted the

460 inflamed areas in red by adjusting the Threshold and measured the areas based on pixel. The percentages
461 of disrupted and inflamed lung areas were calculated based on the ratio of highlighted disrupted areas to
462 the total lung area in each lung section.

463

464 **Western Blot analysis.** Same numbers of cultured or FACS-sorted AM were lysed in lysis buffer
465 (62.5mM Tris-HCL (pH 6.8), 2% SDS and 10% glycerol) with a protease inhibitor cocktail (Roche). The
466 lysates were then separated by SDS-PAGE and transferred to Immuno-Blot Nitrocellulose Membrane
467 (Bio-Rad,). The membranes were blocked with 5% non-fat milk in 20 mM Tris (pH 7.5), 0.5 M NaCl and
468 0.05% Tween 20 (TBST) for 1h at room temperature (RT), followed by incubation with primary Ab
469 against PPAR- γ (1:1000, Cell Signaling Technology) or β -actin (1:5000, Santa Cruz Biotechnology)
470 overnight at 4°C. After washing with TBST buffer, membranes were incubated with goat anti-rabbit or
471 anti-mouse secondary Ab (Promega). Peroxidase activity was detected with enhanced
472 chemiluminescence (ECL).

473

474 **Chromatin Immunoprecipitation (ChIP).** AM were obtained from the lung of naïve WT C57BL6 mice,
475 using anti-CD169 magnetic beads, as recommended by the manufacturer (Miltenyi Biotec). AM were
476 cultured in complete medium supplemented with 10 ng/ml GM-CSF in the presence of 50 ng/ml IFN- α
477 (BioLegend) or vehicle overnight. Then the cells were subjected to ChIP assay as previously described
478 (54). In brief, 8×10^6 AM were crosslinked for 10 min at 37°C by the addition of 1% freshly made
479 formaldehyde. Fixed cells were pelleted at 4°C and washed with ice-cold PBS. The cells were lysed with
480 SDS lysis buffer (1% SDS, 10mM EDTA, 50mM Tris, pH 8.1) containing protease inhibitors (Roche) on
481 ice for 10 min and sonicated to an average size of 200-500bp. After sonication, samples were centrifuged
482 at 13,000 rpm for 10 min at 4°C and 5% of sonicated cell extracts were saved as input. The resulting
483 whole-cell extract was incubated with Protein A/G Agarose (Santa Cruz) for 1h at 4°C. Precleared extracts
484 were then incubated with 60 μ l of Protein A/G Agarose (Santa Cruz) for ChIP with 5 μ g of the appropriate
485 antibody overnight at 4°C. STAT1 ChIP antibody (clone D1K9Y) was from Cell Signaling. After
486 overnight incubation, beads were washed once with low salt immune complex wash buffer (0.1% SDS, 1%
487 Triton X-100, 2 mM EDTA, 20 mM Tris-HCL pH 8.1, 150 mM NaCl), once with high salt immune
488 complex wash buffer (0.1% SDS, 1% Triton X-100, 2 mM EDTA, 20 mM Tris-HCL pH 8.1, 500 mM
489 NaCl), once with LiCl wash buffer (10 mM Tris-HCl pH 8.1, 1 mM EDTA, 250 mM LiCl, 1% NP-40),
490 and twice with TE wash buffer (10 mM Tris-HCl pH 8.0, 1 mM EDTA). DNA was eluted in freshly
491 prepared elution buffer (1% SDS, 0.1M NaHCO₃). Cross-links were reversed by overnight incubation
492 with 5 M NaCl at 65°C. RNA and protein were digested using RNase A and proteinase K (Roche),

493 respectively and DNA was purified by Qiagen MinElute PCR Purification kit according to the
494 manufacturer's instructions. The immunoprecipitated DNA was analyzed by quantitative real-time PCR
495 and normalized relative to input DNA amount. Primers were designed to a segment that was centered on
496 the PPAR- γ coverage regions. Primers used in this study are listed in as follows. Realtime PCR data is
497 represented as fold levels over control. Primers sequence are as following. *Pparg* -4.3k:
498 TGGAATGAAAGAATCCTCCAA, GTTGGTGCCACATGGATTTT. *Pparg* -16.8k:
499 GCAGATTTGTGCCAAGAACA, TGCAGCCGCTGAATAAATAC.

500

501 **ELISA analysis of BAL cytokines.** 50 μ l of each BAL sample was analyzed with the ELISA using
502 commercially available kits for mouse IL-1 β , CCL2 and TNF- α (Biolegend) following the manufacturer's
503 protocol. The VERSAmax microplate reader (Molecular Devices) was used for colorimetric
504 quantification and analysis at 450nm wavelength.

505

506 **BCA protein assay.** BCA protein assay kit was obtained from Thermo Scientific. 2 μ l of each BALF
507 sample was used. VERSAmax microplate reader (Molecular Devices) was used for colorimetric
508 quantification and analysis at 570nm wavelength.

509

510 **Plaque Assay.** IAV plaque assays were performed as described before (55). Briefly, MDCK cells were
511 grown in 6-well plates and incubated with series dilution of BALF for 1 h. The plates were then overlaid
512 with low melting temperature agarose (0.6 %) in MEM with BSA and trypsin and cultured for 3 days in
513 37°C incubator. Plates were then fixed with formaldehyde and virus plaques were visualized with the
514 staining of neutral red.

515

516 **FACS analysis.** Fluorescence-conjugated FACS Abs were purchased from Biolegend, BD Biosciences or
517 eBioscience. Ab clones are provided. We defined cell populations based on following cell surface markers:
518 AM (CD11c⁺ Siglec F⁺ CD11b^{low}), Neutrophils (CD11b⁺ Ly6G⁺), total CD11b⁺ Monocyte/Macrophage
519 population (Ly6G⁻ Siglec F⁻ CD11b⁺), Monocytes (Ly6G⁻ Siglec F⁻ CD11b⁺ Ly6C⁺), NP₃₆₆ tetramer⁺ cells
520 (CD8⁺ NP₃₆₆-tet⁺), PA₂₂₄ tetramer⁺ cells (CD8⁺ PA₂₂₄-tet⁺). Samples were collected on FACS Attune or
521 FACS Attune NXT flow cytometer (Life technologies) and analyzed using Flow Jo software (Tree Star).

522

523 **Statistical analysis.** Data are mean \pm SEM of values from individual mice (*in vivo* experiments).

524 Unpaired two-tailed Student's t-test (two group comparison), Multiple t-tests (weight loss) or Logrank

525 test (survival study) were used to determine statistical significance by GraphPad Prism software. We
526 consider *P* values < 0.05 as significant.

527

528 **ACKNOWLEDGMENTS**

529 We thank Thomas Braciale and Khashayarsha Khazaie for critical reading of the manuscript. We thank
530 NIH tetramer facility for providing IAV-specific tetramers and Mayo flow cytometry core for help of cell
531 sorting. This work was supported by the US National Institutes of Health grants (RO1 HL126647,
532 AG047156, AI112844, R21 AI099753 to J.S.; R01 AI095282 and AI129241 to M.H.K.; RO1 HL62150 to
533 A.H.L.; T32 AG049672 to N.P.G.), Kogod Aging Center High Risk Pilot Grant to J.S. and Huvis
534 Foundation grant to A.H.L.

535

536

537

538

539

540

541

542

543

544

545

546

547

548

549

550

551

552

553

554

555 **REFERENCES**

556

- 557 1. **Openshaw PJM, Chiu C, Culley FJ, Johansson C.** 2017. Protective and Harmful Immunity to RSV Infection.
558 *Annu Rev Immunol* **35**:501-532.

- 559 2. **Zhou H, Thompson WW, Viboud CG, Ringholz CM, Cheng PY, Steiner C, Abedi GR, Anderson LJ, Brammer**
560 **L, Shay DK.** 2012. Hospitalizations associated with influenza and respiratory syncytial virus in the United
561 States, 1993-2008. *Clin Infect Dis* **54**:1427-1436.
- 562 3. **Molinari NA, Ortega-Sanchez IR, Messonnier ML, Thompson WW, Wortley PM, Weintraub E, Bridges CB.**
563 2007. The annual impact of seasonal influenza in the US: measuring disease burden and costs. *Vaccine*
564 **25**:5086-5096.
- 565 4. **Doherty PC, Turner SJ, Webby RG, Thomas PG.** 2006. Influenza and the challenge for immunology. *Nat*
566 *Immunol* **7**:449-455.
- 567 5. **Thomas PG, Keating R, Hulse-Post DJ, Doherty PC.** 2006. Cell-mediated protection in influenza infection.
568 *Emerg Infect Dis* **12**:48-54.
- 569 6. **Hussain M, Galvin HD, Haw TY, Nutsford AN, Husain M.** 2017. Drug resistance in influenza A virus: the
570 epidemiology and management. *Infect Drug Resist* **10**:121-134.
- 571 7. **Braciale TJ, Sun J, Kim TS.** 2012. Regulating the adaptive immune response to respiratory virus infection.
572 *Nat Rev Immunol* **12**:295-305.
- 573 8. **Sun J, Braciale TJ.** 2013. Role of T cell immunity in recovery from influenza virus infection. *Curr Opin Virol*
574 **3**:425-429.
- 575 9. **de Jong MD, Simmons CP, Thanh TT, Hien VM, Smith GJ, Chau TN, Hoang DM, Chau NV, Khanh TH, Dong**
576 **VC, Qui PT, Cam BV, Ha do Q, Guan Y, Peiris JS, Chinh NT, Hien TT, Farrar J.** 2006. Fatal outcome of
577 human influenza A (H5N1) is associated with high viral load and hypercytokinemia. *Nat Med* **12**:1203-
578 1207.
- 579 10. **Kobasa D, Jones SM, Shinya K, Kash JC, Copps J, Ebihara H, Hatta Y, Kim JH, Halfmann P, Hatta M,**
580 **Feldmann F, Alimonti JB, Fernando L, Li Y, Katze MG, Feldmann H, Kawaoka Y.** 2007. Aberrant innate
581 immune response in lethal infection of macaques with the 1918 influenza virus. *Nature* **445**:319-323.
- 582 11. **Lavin Y, Mortha A, Rahman A, Merad M.** 2015. Regulation of macrophage development and function in
583 peripheral tissues. *Nat Rev Immunol* **15**:731-744.
- 584 12. **Geissmann F, Mass E.** 2015. A stratified myeloid system, the challenge of understanding macrophage
585 diversity. *Semin Immunol* **27**:353-356.
- 586 13. **Geissmann F, Gordon S, Hume DA, Mowat AM, Randolph GJ.** 2010. Unravelling mononuclear phagocyte
587 heterogeneity. *Nat Rev Immunol* **10**:453-460.
- 588 14. **Ginhoux F, Guilliams M.** 2016. Tissue-Resident Macrophage Ontogeny and Homeostasis. *Immunity*
589 **44**:439-449.
- 590 15. **Perdiguero EG, Geissmann F.** 2016. The development and maintenance of resident macrophages. *Nat*
591 *Immunol* **17**:2-8.
- 592 16. **Hussell T, Bell TJ.** 2014. Alveolar macrophages: plasticity in a tissue-specific context. *Nat Rev Immunol*
593 **14**:81-93.
- 594 17. **Kopf M, Schneider C, Nobs SP.** 2015. The development and function of lung-resident macrophages and
595 dendritic cells. *Nat Immunol* **16**:36-44.
- 596 18. **Guilliams M, De Kleer I, Henri S, Post S, Vanhoutte L, De Prijck S, Deswarte K, Malissen B, Hammad H,**
597 **Lambrecht BN.** 2013. Alveolar macrophages develop from fetal monocytes that differentiate into long-
598 lived cells in the first week of life via GM-CSF. *J Exp Med* **210**:1977-1992.
- 599 19. **Schneider C, Nobs SP, Kurrer M, Rehrauer H, Thiele C, Kopf M.** 2014. Induction of the nuclear receptor
600 PPAR-gamma by the cytokine GM-CSF is critical for the differentiation of fetal monocytes into alveolar
601 macrophages. *Nat Immunol* **15**:1026-1037.
- 602 20. **Yu X, Buttgereit A, Lelios I, Utz SG, Cansever D, Becher B, Greter M.** 2017. The Cytokine TGF-beta
603 Promotes the Development and Homeostasis of Alveolar Macrophages. *Immunity* **47**:903-912 e904.
- 604 21. **Schneider C, Nobs SP, Heer AK, Hirsch E, Penninger J, Siggs OM, Kopf M.** 2017. Frontline Science:
605 Coincidental null mutation of Csf2ralpha in a colony of PI3Kgamma^{-/-} mice causes alveolar macrophage
606 deficiency and fatal respiratory viral infection. *J Leukoc Biol* **101**:367-376.
- 607 22. **Deng W, Yang J, Lin X, Shin J, Gao J, Zhong XP.** 2017. Essential Role of mTORC1 in Self-Renewal of Murine
608 Alveolar Macrophages. *J Immunol* **198**:492-504.

- 609 23. **Kawasaki T, Ito K, Miyata H, Akira S, Kawai T.** 2017. Deletion of PIKfyve alters alveolar macrophage
610 populations and exacerbates allergic inflammation in mice. *EMBO J* **36**:1707-1718.
- 611 24. **Todd EM, Zhou JY, Szasz TP, Deady LE, D'Angelo JA, Cheung MD, Kim AH, Morley SC.** 2016. Alveolar
612 macrophage development in mice requires L-plastin for cellular localization in alveoli. *Blood* **128**:2785-
613 2796.
- 614 25. **Laidlaw BJ, Decman V, Ali MA, Abt MC, Wolf AI, Monticelli LA, Mozdanzowska K, Angelosanto JM, Artis
615 D, Erikson J, Wherry EJ.** 2013. Cooperativity between CD8+ T cells, non-neutralizing antibodies, and
616 alveolar macrophages is important for heterosubtypic influenza virus immunity. *PLoS Pathog* **9**:e1003207.
- 617 26. **Schneider C, Nobs SP, Heer AK, Kurrer M, Klinke G, van Rooijen N, Vogel J, Kopf M.** 2014. Alveolar
618 macrophages are essential for protection from respiratory failure and associated morbidity following
619 influenza virus infection. *PLoS Pathog* **10**:e1004053.
- 620 27. **Kim HM, Lee YW, Lee KJ, Kim HS, Cho SW, van Rooijen N, Guan Y, Seo SH.** 2008. Alveolar macrophages
621 are indispensable for controlling influenza viruses in lungs of pigs. *J Virol* **82**:4265-4274.
- 622 28. **Purnama C, Ng SL, Tetlak P, Setiagani YA, Kandasamy M, Baalashubramanian S, Karjalainen K, Ruedl C.**
623 2014. Transient ablation of alveolar macrophages leads to massive pathology of influenza infection
624 without affecting cellular adaptive immunity. *Eur J Immunol* **44**:2003-2012.
- 625 29. **Kumagai Y, Takeuchi O, Kato H, Kumar H, Matsui K, Morii E, Aozasa K, Kawai T, Akira S.** 2007. Alveolar
626 macrophages are the primary interferon-alpha producer in pulmonary infection with RNA viruses.
627 *Immunity* **27**:240-252.
- 628 30. **Cardani A, Boulton A, Kim TS, Braciale TJ.** 2017. Alveolar Macrophages Prevent Lethal Influenza
629 Pneumonia By Inhibiting Infection Of Type-1 Alveolar Epithelial Cells. *PLoS Pathog* **13**:e1006140.
- 630 31. **Goritzka M, Makris S, Kausar F, Durant LR, Pereira C, Kumagai Y, Culley FJ, Mack M, Akira S, Johansson C.**
631 2015. Alveolar macrophage-derived type I interferons orchestrate innate immunity to RSV through
632 recruitment of antiviral monocytes. *J Exp Med* **212**:699-714.
- 633 32. **Gorski SA, Hufford MM, Braciale TJ.** 2012. Recent insights into pulmonary repair following virus-induced
634 inflammation of the respiratory tract. *Curr Opin Virol* **2**:233-241.
- 635 33. **Ahmadian M, Suh JM, Hah N, Liddle C, Atkins AR, Downes M, Evans RM.** 2013. PPARgamma signaling
636 and metabolism: the good, the bad and the future. *Nat Med* **19**:557-566.
- 637 34. **Odegaard JI, Ricardo-Gonzalez RR, Goforth MH, Morel CR, Subramanian V, Mukundan L, Red Eagle A,
638 Vats D, Brombacher F, Ferrante AW, Chawla A.** 2007. Macrophage-specific PPARgamma controls
639 alternative activation and improves insulin resistance. *Nature* **447**:1116-1120.
- 640 35. **Chawla A.** 2010. Control of macrophage activation and function by PPARs. *Circ Res* **106**:1559-1569.
- 641 36. **Moseley CE, Webster RG, Aldridge JR.** 2010. Peroxisome proliferator-activated receptor and AMP-
642 activated protein kinase agonists protect against lethal influenza virus challenge in mice. *Influenza Other
643 Respir Viruses* **4**:307-311.
- 644 37. **Darwish I, Mubareka S, Liles WC.** 2011. Immunomodulatory therapy for severe influenza. *Expert Rev Anti
645 Infect Ther* **9**:807-822.
- 646 38. **Cloutier A, Marois I, Cloutier D, Verreault C, Cantin AM, Richter MV.** 2012. The prostanoid 15-deoxy-
647 Delta12,14-prostaglandin-j2 reduces lung inflammation and protects mice against lethal influenza
648 infection. *J Infect Dis* **205**:621-630.
- 649 39. **Fedson DS.** 2013. Treating influenza with statins and other immunomodulatory agents. *Antiviral Res*
650 **99**:417-435.
- 651 40. **Aldridge JR, Jr., Moseley CE, Boltz DA, Negovetich NJ, Reynolds C, Franks J, Brown SA, Doherty PC,
652 Webster RG, Thomas PG.** 2009. TNF/iNOS-producing dendritic cells are the necessary evil of lethal
653 influenza virus infection. *Proc Natl Acad Sci U S A* **106**:5306-5311.
- 654 41. **Herold S, Steinmueller M, von Wulffen W, Cakarova L, Pinto R, Pleschka S, Mack M, Kuziel WA, Corazza
655 N, Brunner T, Seeger W, Lohmeyer J.** 2008. Lung epithelial apoptosis in influenza virus pneumonia: the
656 role of macrophage-expressed TNF-related apoptosis-inducing ligand. *J Exp Med* **205**:3065-3077.
- 657 42. **Lin KL, Suzuki Y, Nakano H, Ramsburg E, Gunn MD.** 2008. CCR2+ monocyte-derived dendritic cells and
658 exudate macrophages produce influenza-induced pulmonary immune pathology and mortality. *J Immunol*
659 **180**:2562-2572.

- 660 43. **Hashimoto D, Chow A, Noizat C, Teo P, Beasley MB, Leboeuf M, Becker CD, See P, Price J, Lucas D,**
661 **Greter M, Mortha A, Boyer SW, Forsberg EC, Tanaka M, van Rooijen N, Garcia-Sastre A, Stanley ER,**
662 **Ginhoux F, Frenette PS, Merad M.** 2013. Tissue-resident macrophages self-maintain locally throughout
663 adult life with minimal contribution from circulating monocytes. *Immunity* **38**:792-804.
- 664 44. **Channappanavar R, Fehr AR, Vijay R, Mack M, Zhao J, Meyerholz DK, Perlman S.** 2016. Dysregulated
665 Type I Interferon and Inflammatory Monocyte-Macrophage Responses Cause Lethal Pneumonia in SARS-
666 CoV-Infected Mice. *Cell Host Microbe* **19**:181-193.
- 667 45. **Gautier EL, Chow A, Spanbroek R, Marcelin G, Greter M, Jakubzick C, Bogunovic M, Leboeuf M, van**
668 **Rooijen N, Habenicht AJ, Merad M, Randolph GJ.** 2012. Systemic analysis of PPARgamma in mouse
669 macrophage populations reveals marked diversity in expression with critical roles in resolution of
670 inflammation and airway immunity. *J Immunol* **189**:2614-2624.
- 671 46. **Ichinohe T, Pang IK, Kumamoto Y, Peaper DR, Ho JH, Murray TS, Iwasaki A.** 2011. Microbiota regulates
672 immune defense against respiratory tract influenza A virus infection. *Proc Natl Acad Sci U S A* **108**:5354-
673 5359.
- 674 47. **Garcia-Sastre A, Biron CA.** 2006. Type 1 interferons and the virus-host relationship: a lesson in detente.
675 *Science* **312**:879-882.
- 676 48. **Teijaro JR, Walsh KB, Cahalan S, Fremgen DM, Roberts E, Scott F, Martinborough E, Peach R, Oldstone**
677 **MB, Rosen H.** 2011. Endothelial cells are central orchestrators of cytokine amplification during influenza
678 virus infection. *Cell* **146**:980-991.
- 679 49. **Teijaro JR.** 2015. The role of cytokine responses during influenza virus pathogenesis and potential
680 therapeutic options. *Curr Top Microbiol Immunol* **386**:3-22.
- 681 50. **Davidson S, Crotta S, McCabe TM, Wack A.** 2014. Pathogenic potential of interferon alphabeta in acute
682 influenza infection. *Nat Commun* **5**:3864.
- 683 51. **Sun J, Madan R, Karp CL, Braciale TJ.** 2009. Effector T cells control lung inflammation during acute
684 influenza virus infection by producing IL-10. *Nat Med* **15**:277-284.
- 685 52. **Yao S, Jiang L, Moser EK, Jewett LB, Wright J, Du J, Zhou B, Davis SD, Krupp NL, Braciale TJ, Sun J.** 2015.
686 Control of pathogenic effector T-cell activities in situ by PD-L1 expression on respiratory inflammatory
687 dendritic cells during respiratory syncytial virus infection. *Mucosal Immunol* **8**:746-759.
- 688 53. **Mack M, Cihak J, Simonis C, Luckow B, Proudfoot AE, Plachy J, Bruhl H, Frink M, Anders HJ, Vielhauer V,**
689 **Pfirstinger J, Stangassinger M, Schlondorff D.** 2001. Expression and characterization of the chemokine
690 receptors CCR2 and CCR5 in mice. *J Immunol* **166**:4697-4704.
- 691 54. **Yao S, Buzo BF, Pham D, Jiang L, Taparowsky EJ, Kaplan MH, Sun J.** 2013. Interferon regulatory factor 4
692 sustains CD8(+) T cell expansion and effector differentiation. *Immunity* **39**:833-845.
- 693 55. **Huprikar J, Rabinowitz S.** 1980. A simplified plaque assay for influenza viruses in Madin-Darby kidney
694 (MDCK) cells. *J Virol Methods* **1**:117-120.
- 695
696
697
698
699
700
701
702
703

704 FIGURE LEGENDS

705 **Figure 1. IAV down-regulates PPAR- γ expression in AM.**

- 706 A. Comparison of the expression of 84 transcription factors in AM (isolated and pooled from at least
707 3 mice) with or without IAV (IAV) infection for overnight *in vitro* by RT² Profiler PCR array.
708 Dotted line: fold cutoff of gene expression (1.5 fold). Red dots, genes up-regulated following IAV
709 infection. Green dots, genes down-regulated following IAV infection.
- 710 B. List of up- or down-regulated transcription factors in AM (isolated and pooled from at least 3
711 mice) following IAV infection *in vitro* for overnight by RT² Profiler PCR array.
- 712 C. Relative expression of *Pparg* in AM (isolated and pooled from at least 3 mice) with or without
713 IAV infection for overnight *in vitro* by qRT-PCR.
- 714 D. Western blot analysis of PPAR- γ levels in AM (isolated and pooled from at least 3 mice) with or
715 without IAV infection for overnight. Bar graph represents relative density of PPAR- γ band pooled
716 from three independent experiments.
- 717 E. Relative expression of *Pparg* in sorted AM isolated from non-infected (day 0) or IAV-infected
718 mice at 4, 6, 10 or 15 p.i.
- 719 F. Western blot analysis of PPAR- γ expression *ex vivo* in AM (isolated and pooled from at least 3
720 mice) isolated from non-infected (day 0) or IAV-infected lungs (6 d.p.i.). Bar graphs represent
721 relative density of PPAR- γ band pooled from three independent experiments.
- 722 G. Western blot analysis of PPAR- γ expression in AM (isolated and pooled from at least 3 mice) with
723 or without IFN- α treatment for overnight. Bar graph represent relative density of PPAR- γ band
724 pooled from three independent experiments.
- 725 H. Relative expression of *Pparg* in AM (isolated and pooled from at least 3 mice) with or without
726 IAV infection in the presence or absence of α -IFNAR1 for overnight *in vitro* by qRT-PCR.
- 727 I. STAT1 binding to *Pparg* locus in AM following overnight IFN- α treatment *in vitro* was
728 determined through CHIP (pooled from n>20 mice). Numbers in Red are distances of the binding
729 sites to start codon.

730 Data are representative of two to three independent experiments. *, P < 0.05.

731

732 **Figure 2. PPAR- γ suppresses antiviral inflammation, but not regulates M2 genes following infection**

- 733 A. Airway AM percentages and CD11b expression on AM from control (*Pparg*^{fl/fl}) or *Pparg*^{ACD11c}
734 mice, and control or *Pparg*^{ALyz2} mice.
- 735 B. Western blot of PPAR- γ expression in sorted AM (isolated and pooled from 2-3 mice) from
736 control (*Pparg*^{fl/fl}) or *Pparg*^{ALyz2} mice at 0 and 3 d.p.i.

- 737 C. qRT-PCR analysis of *Ifna4*, *Ifnb1*, *Il1b*, *Tnf*, *Ccl2*, *Retnla* and *Arg1* expression in AM (isolated
738 and pooled from 3 mice) from control (*Pparg^{fl/fl}*) or *Pparg^{ALyz2}* mice following IAV infection *in*
739 *vitro* for overnight.
- 740 D. Control or *Pparg^{ALyz2}* mice were infected with IAV. *Ifna4*, *Ifnb1*, *Tnf*, *Ccl2*, *Retnla* and *Arg1* gene
741 expression in AM (isolated and pooled from 2-3 mice) of control or *Pparg^{ALyz2}* mice at day 1 and 3
742 p.i.

743 Data are representative of at least two independent experiments. *, $P < 0.05$.

744

745 **Figure 3. Myeloid PPAR- γ suppresses host mortality, morbidity and pulmonary inflammation.**

746 Control or *Pparg^{ALyz2}* mice were infected with IAV.

- 747 A. Host mortality (% survival) was monitored.
- 748 B. Host morbidity (% initial weight) was monitored.
- 749 C. Airway IAV titers (pfu assay) were determined at day 4, 7, 10 or 15 p.i..
- 750 D. Lung IAV-specific PA₂₂₄ and NP₃₆₆ tetramer⁺ CD8⁺ T cells at day 7, 10 and 15 p.i.
- 751 E. CCL2 and TNF- α levels in the BAL were quantified by ELISA at day 1, 3, 7, 10 or 15 p.i.
- 752 F. Comparison of the expression of 84 inflammation-related genes in lungs from control or
753 *Pparg^{ALyz2}* mice at day 10 p.i. by RT² Profiler PCR array. Dotted line: 1.5 fold difference cutoff.
754 Red dots, genes up-regulated in the lungs of *Pparg^{ALyz2}* mice. Green dots, genes down-regulated in
755 the lungs of *Pparg^{ALyz2}* mice.

756 Data are representative of at least two independent experiments (n=3-6 mice per group) except A, B,
757 C (pooled data from 2-6 experiments). *, $P < 0.05$.

758

759 **Figure 4. Myeloid PPAR- γ suppresses pulmonary inflammation during RSV infection.**

- 760 A. qRT-PCR analysis of *Ifna4*, *Ifnb1*, *Il1b*, *Tnf*, *Ccl2*, *Retnla* and *Arg1* expression in AM (isolated
761 and pooled from at least 3 mice) from control (*Pparg^{fl/fl}*) or *Pparg^{ALyz2}* mice following RSV
762 infection (10 MOI) *in vitro* for overnight.
- 763 B-D. Control (*Pparg^{fl/fl}*) or *Pparg^{ALyz2}* mice were infected with RSV.
- 764 B. Host morbidity (% initial weight) was monitored daily.
- 765 C. Numbers of lung neutrophils or monocytes at 4 d.p.i.
- 766 D. BAL TNF and IL-1 β concentrations were determined through ELISA at 4 d.p.i.

767 Data are representative of at least two independent experiments (n=3-4 mice per group) except B
768 (pooled data from 2 experiments). *, $P < 0.05$.

769

770 **Figure 5. PPAR- γ expression in resident alveolar macrophages is likely required for the suppression**
771 **of host morbidity**

- 772 A. *Lyz2*-cre gene recombination in AM, neutrophils and CD11b⁺ monocytes/macrophages is reported
773 by % eYFP expression following crossing with R26R-eYFP reporter mice.
774 B. Western blot analysis of PPAR- γ protein expression in sorted AM, CD11b⁺
775 monocytes/macrophages and neutrophils in the lungs from naïve WT mice (pooled from 3 mice).
776 C. *Tnf* and *Ccl2* expression in indicated cell populations in the lungs of control (*Pparg*^{fl/fl}) or
777 *Pparg*^{ALyz2} mice at day 1 and 3 p.i. (pooled from 2-3 mice per group).
778 D. *Ccr2*^{-/-} *Pparg*^{fl/fl} and *Ccr2*^{-/-} *Pparg*^{ALyz2} mice were infected with IAV. Host morbidity (% initial
779 weight) was monitored.
780 E. WT mice were infected with IAV and treated with control IgG or MC21 mAb. % lung AM (upper
781 panel) and monocytes (lower panel) in CD45⁺ Ly6G⁻ cells are depicted at 5 d.p.i.
782 F. Control (*Pparg*^{fl/fl}) and *Pparg*^{ALyz2} mice were infected with IAV and treated with control IgG or
783 MC21 mAb. Host morbidity (% initial weight) was monitored.
784 Data are representative of at least two to three independent experiments except C (pooled data from 3
785 experiments) and D. *, *P* < 0.05.

787 **Figure 6. Macrophage PPAR- γ modulates inflammation resolution and tissue repair.**

- 788 A. Comparison of the expression of 84 wound healing genes of AM isolated (pooled from 3 mice)
789 from uninfected control or *Pparg*^{ALyz2} mice *in vitro*. Dotted line: fold cutoff of gene expression
790 (1.5 fold). Red dots, genes up-regulated in PPAR- γ -deficient AM. Green dots, genes down-
791 regulated in PPAR- γ -deficient AM.
792 B. List of up- or down-regulated wound healing genes in AM (pooled from 3 mice) from control or
793 *Pparg*^{ALyz2} mice by RT² Profiler PCR array.
794 C-F. Control (*Pparg*^{fl/fl}) or *Pparg*^{ALyz2} mice were infected with IAV (n=3-4).
795 C. H&E staining of lung sections of control or *Pparg*^{ALyz2} mice at day 15 p.i. Left panel,
796 representative images. Right panel, quantification of percentages of inflamed and disrupted
797 alveolar area in the lungs of control (*Pparg*^{fl/fl}) and *Pparg*^{ALyz2} mice.
798 D. BAL neutrophil or monocyte numbers were enumerated at 15 d.p.i.
799 E. BAL total protein concentrations were determined at 1, 3, 7, 10 or 15 d.p.i.
800 F. *Sftpb* and *Abca3* gene expression in lungs from control or *Pparg*^{ALyz2} mice at 8, 10 or 15 d.p.i.
801 Data are representative of at least two independent experiments, *, *P* < 0.05.

802

Figure 1

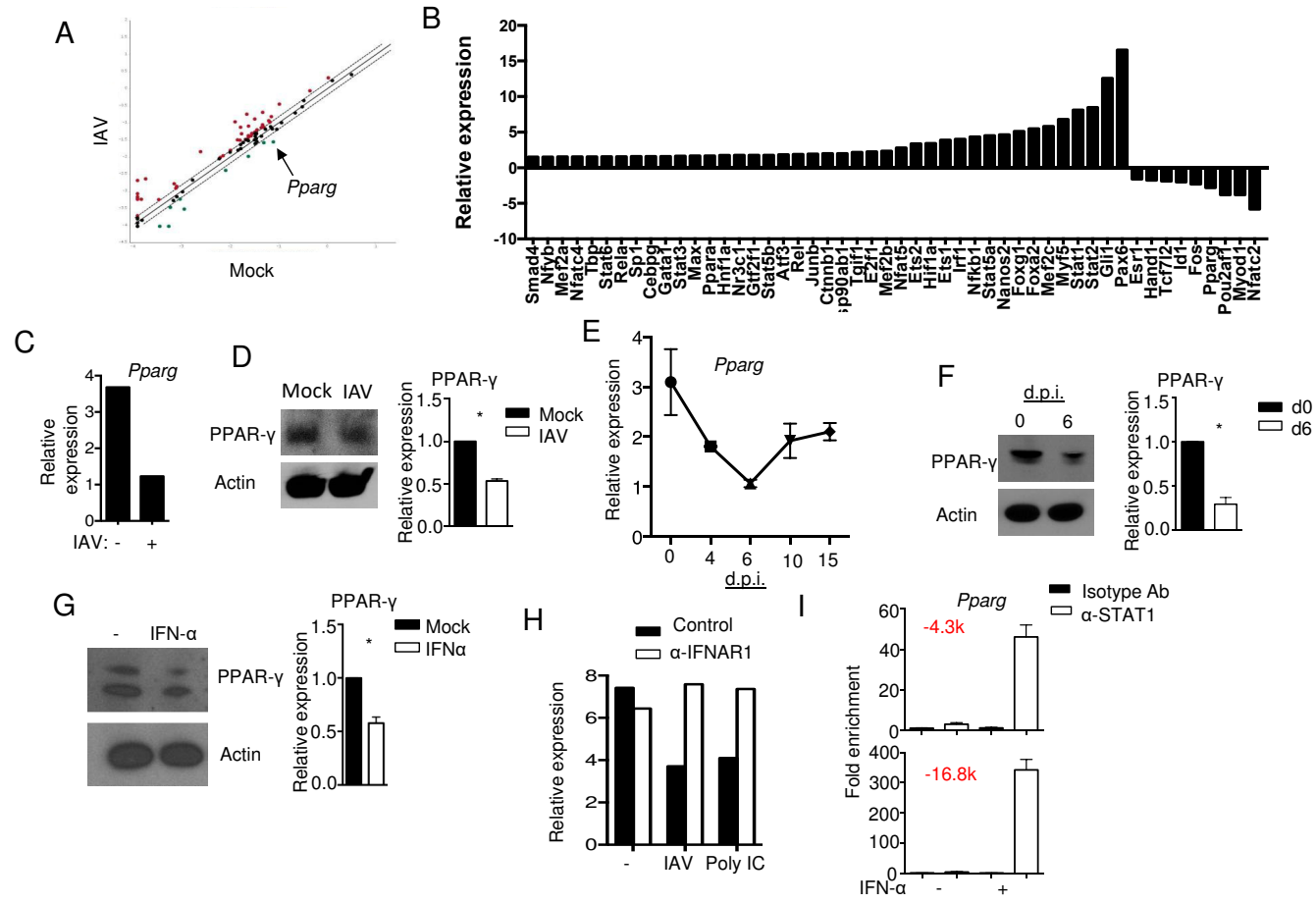


Figure 2

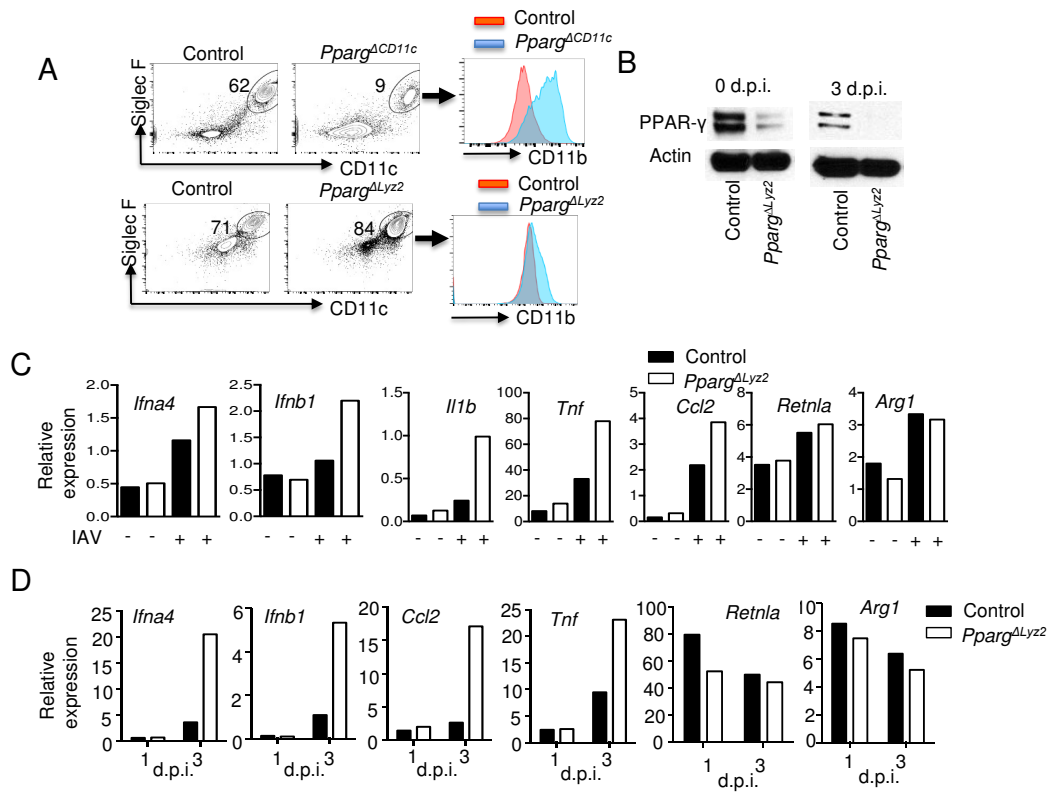


Figure 3

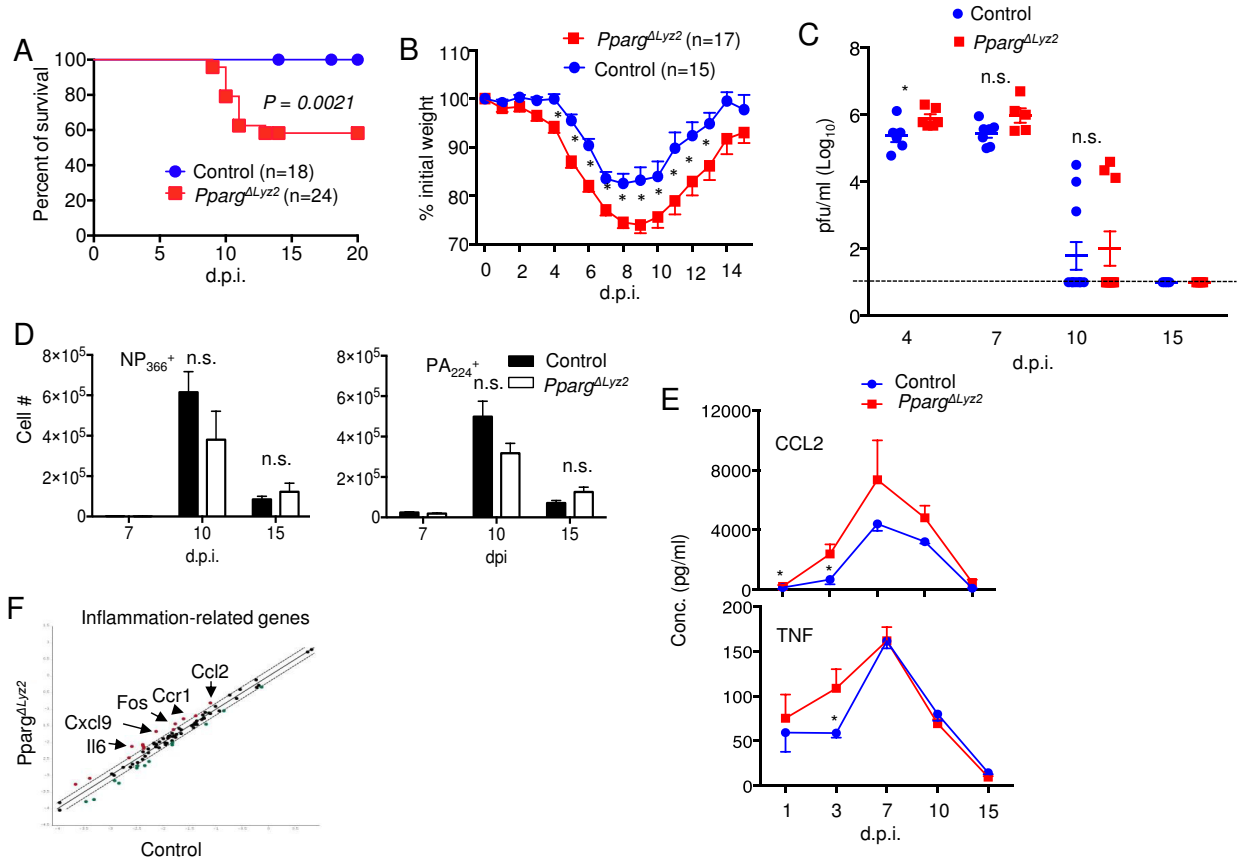


Figure 4

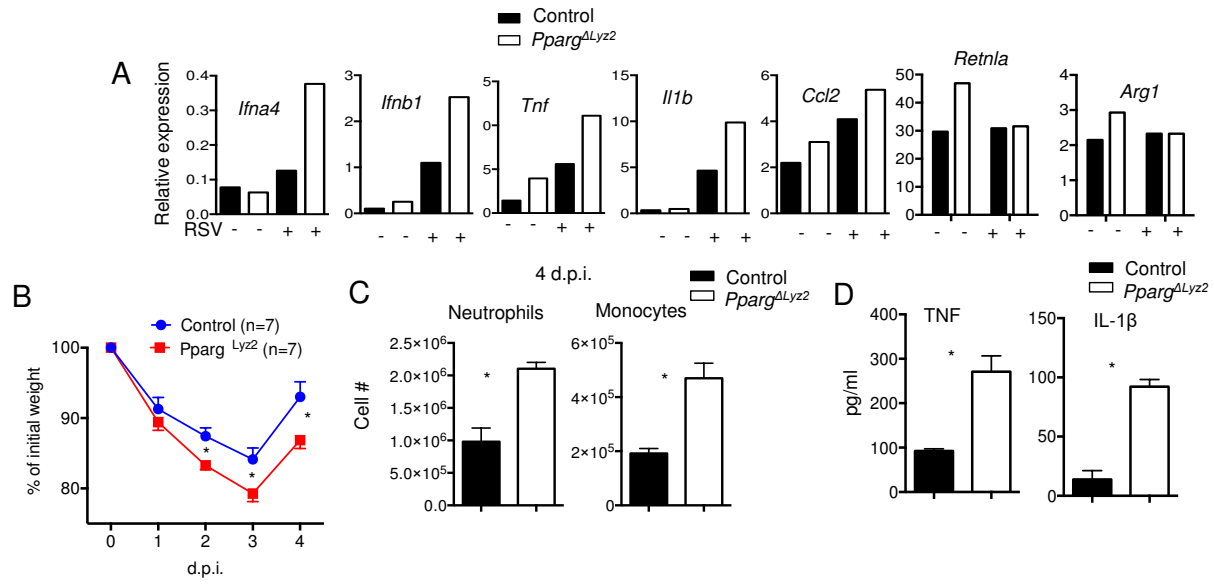


Figure 5

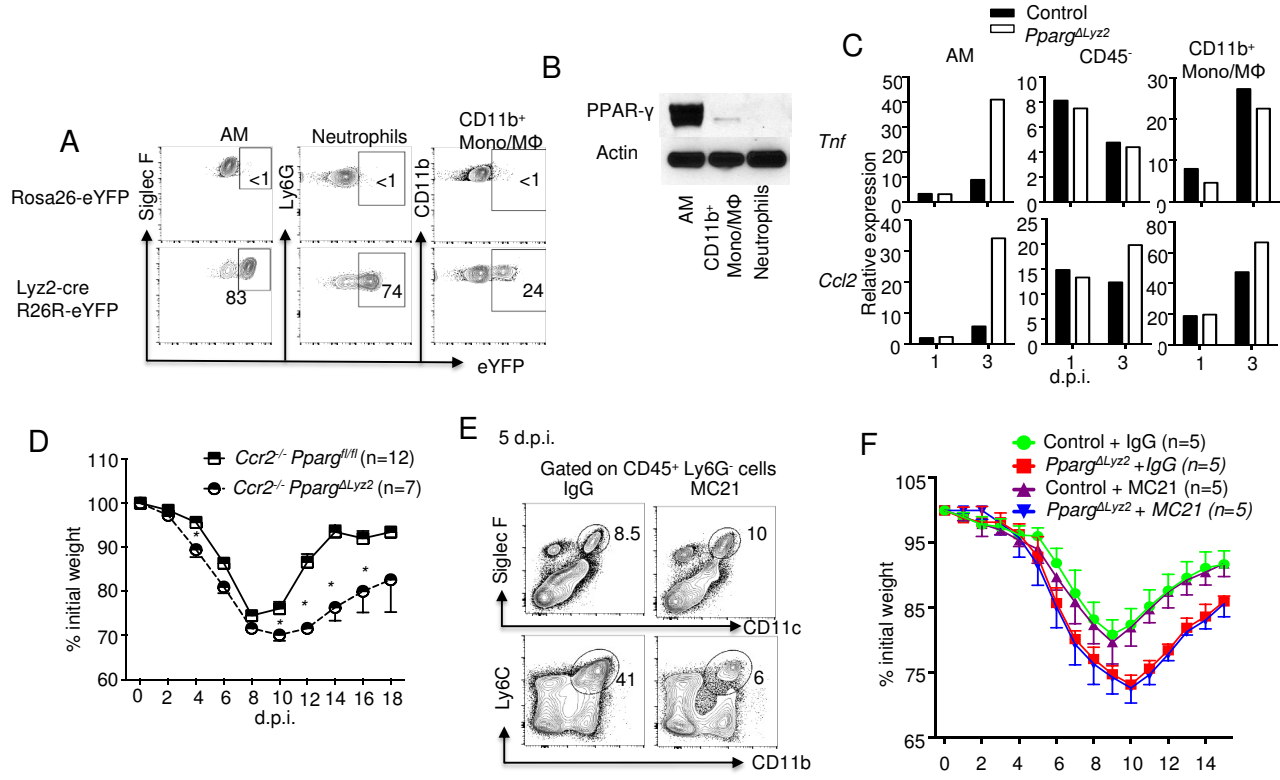


Figure 6

